Rosacea Is Characterized by a Profoundly Diminished Skin Barrier

*JID*Open

Barbara Medgyesi[1,2,3,7], Zsolt Dajnoki[1,2,7], Gabriella Béke[1,2], Krisztián Gáspár[1,2], Imre Lőrinc Szabó[1,2], Eszter Anna Janka[2], Szilárd Póliska[4], Zoltán Hendrik[5], Gábor Méhes[5], Dániel Törőcsik[2], Tamás Bíró[6], Anikó Kapitány[1,2,8] and Andrea Szegedi[1,2,8]

Rosacea is a common chronic inflammation of sebaceous gland–rich facial skin characterized by severe skin dryness, elevated pH, transepidermal water loss, and decreased hydration levels. Until now, there has been no thorough molecular analysis of permeability barrier alterations in the skin of patients with rosacea. Thus, we aimed to investigate the barrier alterations in papulopustular rosacea samples compared with healthy sebaceous gland–rich skin, using RNA sequencing analysis (n = 8). Pathway analyses by Cytoscape ClueGO revealed 15 significantly enriched pathways related to skin barrier formation. RT-PCR and immunohistochemistry were used to validate the pathway analyses. The results showed significant alterations in barrier components in papulopustular rosacea samples compared with sebaceous gland–rich skin, including the cornified envelope and intercellular lipid lamellae formation, desmosome and tight junction organizations, barrier alarmins, and antimicrobial peptides. Moreover, the barrier damage in papulopustular rosacea was unexpectedly similar to atopic dermatitis; this similarity was confirmed by immunofluorescent staining. In summary, besides the well-known dysregulation of immunological, vascular, and neurological functions, we demonstrated prominent permeability barrier alterations in papulopustular rosacea at the molecular level, which highlight the importance of barrier repair therapies for rosacea.

INTRODUCTION

Rosacea is a common chronic immune-mediated inflammatory skin disease of unknown cause (Buhl et al., 2015; Gallo et al., 2018a; Steinhoff et al., 2011). Rosacea mainly affects sebaceous gland–rich (SGR) skin regions, particularly the central face, nose, chin, and forehead of light-skinned people, aged 30–50 years (Buechner, 2005). The prevalence of rosacea in Europe is 2–10% (Gallo et al., 2018b). Clinical features of rosacea include flushing (transient erythema), persistent erythema, telangiectasia, papules, pustules, plaques, edema, and phyma (Gallo et al., 2018b). The four major clinical subtypes of rosacea are erythematotelangiectatic, phymatous, ocular, and papulopustular rosacea (PPR) (Crawford et al., 2004; Gallo et al., 2018b).

Although rosacea occurs in SGR skin regions, affected skin of patients is frequently observed as severely dry and sensitive by dermatologists. Moreover, several functional studies indicate that the skin permeability barrier is dysfunctional in rosacea. The lesional skin of patients is characterized by significantly increased pH and transepidermal water loss, whereas skin hydration levels are significantly decreased (Darlenski et al., 2013; Powell and Ni Raghallaigh, 2011). Although recent studies demonstrate that a dysfunctional barrier is capable of either initiating or augmenting inflammatory skin diseases, barrier damage in the skin of patients with rosacea has not been thoroughly investigated.

Therefore, in this study, in the lesional skin of patients suffering from PPR, we characterized the major groups of molecules involved in permeability barrier formation including cornified envelope and intercellular lipid lamellae formation, desmosome and tight junction organizations, barrier alarmins, and antimicrobial peptides (AMPs). We performed whole transcriptomic analysis using RNA sequencing (RNASeq) and confirmed our results with quantitative real-time reverse transcriptase–PCR and immunohistochemistry (IHC). In addition, we compared PPR barrier damage to that of atopic dermatitis (AD), another inflammatory skin disease with a well-described dysfunctional skin barrier. Because different healthy skin regions have unique immune and barrier characteristics, exclusively SGR skin was

[1]Division of Dermatological Allergology, Department of Dermatology, Faculty of Medicine, University of Debrecen, Debrecen, Hungary; [2]Department of Dermatology, Faculty of Medicine, University of Debrecen, Debrecen, Hungary; [3]Doctoral School of Clinical Immunology and Allergology, University of Debrecen, Debrecen, Hungary; [4]Genomic Medicine and Bioinformatics Core Facility, Department of Biochemistry and Molecular Biology, Faculty of Medicine, University of Debrecen, Debrecen, Hungary; [5]Department of Pathology, Faculty of Medicine, University of Debrecen, Debrecen, Hungary; and [6]Department of Immunology, Faculty of Medicine, University of Debrecen, Debrecen, Hungary

[7]These authors contributed equally to this work.

[8]These authors contributed equally to this work.

Correspondence: Andrea Szegedi, Division of Dermatological Allergology, Department of Dermatology, Faculty of Medicine, University of Debrecen, Hungary, 4032, Nagyerdei street 98, Debrecen, Hungary. E-mail: aszegedi@med.unideb.hu

used as a healthy control for comparison with PPR specimens (Béke et al., 2018; Dajnoki et al., 2017; Jenei et al., 2019).

According to our results, all major components of the skin permeability barrier in patients with PPR were severely affected and were unexpectedly similar to that of affected AD skin. To confirm the similarities between the two inflammatory skin diseases, we performed immunofluorescent staining on selected molecules important in the formation of the permeability skin barrier. Our findings also highlight the importance of skin barrier restoring therapies for the management of rosacea. Based on our results, we recommend the incorporation of skin barrier targeted therapies into clinical guidelines for rosacea, similar to the recommendations for AD.

RESULTS
RNASeq reveals prominent barrier differences between PPR and SGR skin samples

Heatmap, principal component analysis. To identify the in-depth differences in gene expression patterns between SGR and PPR skin samples, RNASeq analysis was performed on lysates of eight healthy SGR skin samples and eight PPR samples. The PPR and SGR sample groups were clearly separated in the heatmap as well as in the principal component analysis of the RNASeq data (Figure 1a and b). The following statistical cut-off level was applied: a minimum of 1.5-fold alteration (fold change; higher or lower levels in PPR over SGR) in the average expression of the given molecular transcript in all donors at $P < 0.05$ statistical significance. A total of 5,136 genes were differentially expressed in PPR compared with SGR skin. Of the differentially expressed genes (DEGs), 3,133 genes showed higher expression, whereas 2,003 genes were expressed at lower levels in PPR as compared with SGR (Supplementary Table S1).

Pathway analysis 1. To identify the function of the DEGs, multiple bioinformatics analyses were performed using the Cytoscape ClueGO bioinformatics tool (Bindea et al., 2009). First, to identify the general biological function of DEGs, we performed a pathway enrichment analysis on all DEGs with fold change ≥ 1.5. To identify the significantly enriched ($P \leq 0.05$) terms and/or pathways with global functions, the following criterion was applied: all terms contain at least 50 genes from our input gene set (the detailed parameters of the analysis can be found in the Materials and Methods section). By using the above approach, 1,239 significantly enriched terms were found by ClueGO. Unsurprisingly, the identified terms were mostly involved in cellular/metabolic functions (e.g., ion transport, lipid biosynthetic process, and transferase activity) and innate (e.g., response to external stimulus, response to stress, cytokine secretion, defense response to bacterium, NOD-like receptor signaling pathway, and complement activation) and adaptive (e.g., T-cell activation, leukocyte migration, TNF production, IFN-gamma production, and chemokine signaling pathway) immune mechanisms. In addition, genes taking part in vascularization (e.g., regulation of vasculature development and angiogenesis) and the nervous system (e.g., nervous system development) were differentially expressed (Figure 1c, Supplementary Table S2). Most importantly, 24 terms related to skin barrier were also

differentially expressed (e.g., epithelium development, morphogenesis of an epithelium, epithelial cell differentiation, and epithelial cell proliferation) (Figure 1c, Supplementary Table S2).

Pathway analysis 2. Next, we performed a second pathway enrichment analysis to determine the specific functions of DEGs; thus, a stricter analytical approach was applied and the up- and downregulated DEGs were analyzed as two different clusters by ClueGO (the detailed parameters of the analysis can be found in the Materials and Methods section). This analytical approach revealed 426 significantly enriched terms and/or pathways (Supplementary Table S3) and most of them (291) belonged to innate and adaptive immune mechanisms (e.g., T helper type [Th] 17 cell differentiation, toll-like receptor cascades, T-cell selection, and neutrophil migration). In addition, several terms were involved in cellular and metabolic functions (63 terms; e.g., transport along microtubule, exocytosis of specific granule membrane proteins, and response to cAMP) and took part in vascularization (2 terms; positive regulation of vasculature development and positive regulation of angiogenesis) and the nervous system (21 terms; e.g., axonogenesis, glial cell differentiation, and axon guidance) were differentially expressed (Supplementary Table S3). Notably, 15 terms were found to be related to skin barrier function (e.g., keratinization, cornification, and tight junction) (Figure 1d and e, Supplementary Table S3). Hereafter, we focused on the skin barrier-related pathways (Figure 1d).

RT-qPCR and IHC validation confirm the significant alterations in the major skin barrier components in PPR

To gain further insight into the permeability barrier differences in PPR versus healthy SGR skin, we examined the expression of genes belonging to the major groups of skin barrier molecules by RT-qPCR. These major groups included (i) cornified envelope formation (FLG, KRT1, KRT10, LCE1D, LCE1F, LOR, SPRR1A, SPRR2A, TGM1, TGM3, and TGM5), (ii) intercellular lipid lamellae formation (ABCA12), (iii) desmosome organization (CDH1, corneodesmosin [CDSN], desmoglein 1 [DSG1], DSC1, and PKP1), (iv) corneocyte desquamation (kallikrein [KLK]5, KLK7, and KLK14), (v) tight junction formation (CLDN1, CLDN16, CLDN23, and OCLN), (vi) barrier alarmins (KRT6, KRT16, and KRT17), and (vii) AMPs (S100A7, S100A8, S100A9, DEFB4B, LCN2, and cathelicidin). Furthermore, we also assessed the expression of selected molecules at the protein level by using IHC.

Cornified envelope formation. First, we focused on investigating the mRNA levels of molecules composing the cornified envelope in healthy SGR and PPR skin samples. Using RT-qPCR, we verified the RNASeq results. Most structural molecules (*KRT1, KRT10, FLG, LOR, LCE1D,* and *LCE1F*) were downregulated in PPR samples, whereas *SPRR1A* and *SPRR2A* mRNA levels were higher in the diseased samples compared with the healthy controls (Table 1, Supplementary Figure S1). The differences were statistically significant in all cases, except for *LCE1D, LCE1F,* and *SPRR1A*. Enzymes crucial for peptide cross-linking (*TGM1* and *TGM3*) were expressed at similar levels in PPR and SGR samples, except for *TGM5*. *TGM5* was significantly downregulated in PPR
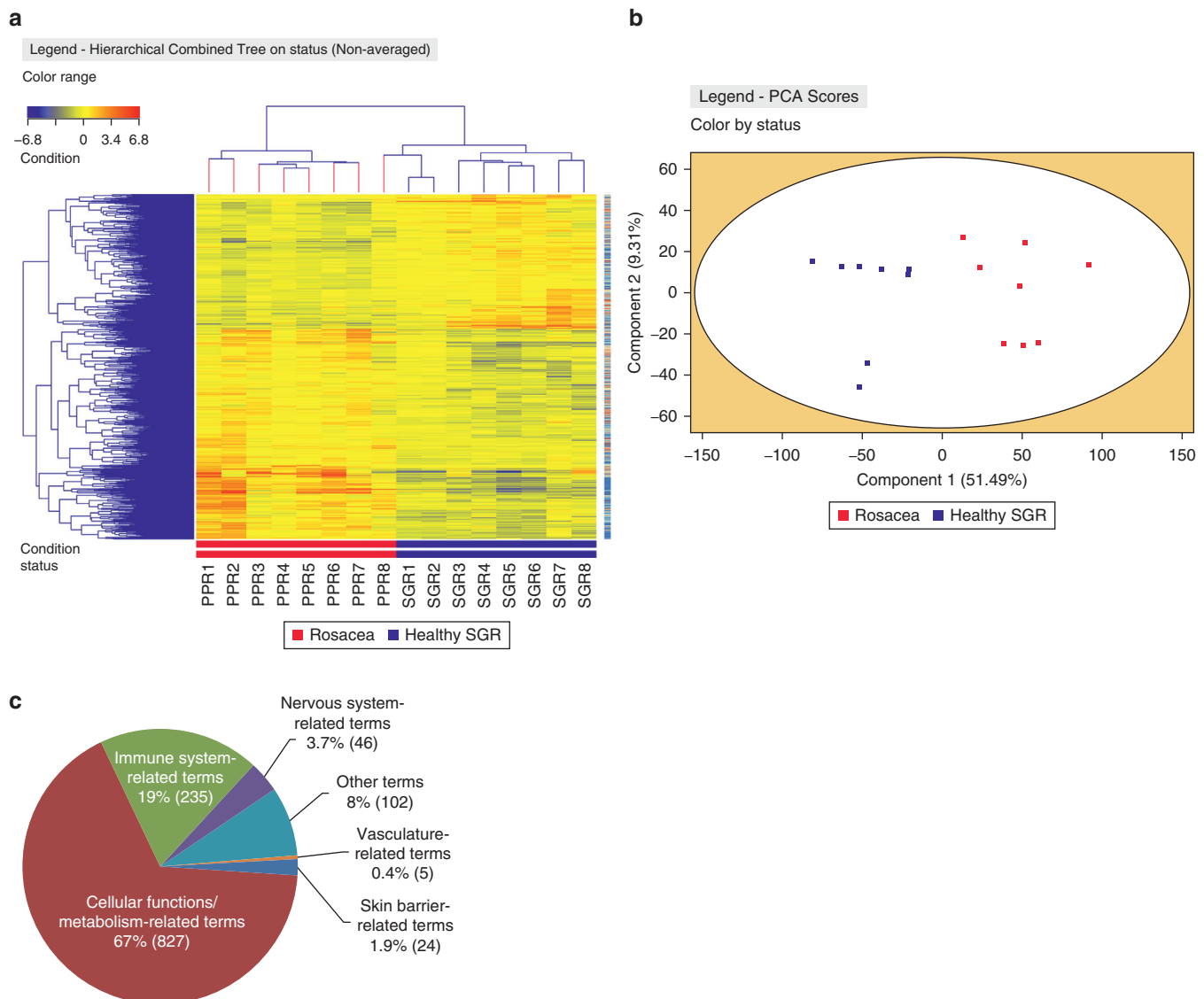
Figure 1. RNASeq analyses revealed significant skin barrier−related differences between PPR and healthy SGR skin samples. (a) Heat map was created by analyzing genes showing significantly different expression ($P < 0.05$) between SGR (n = 8) and PPR (n = 8) skin. (b) Principal component analysis generated by StrandNGS software could distinguish the two sample groups unambiguously. (c) The distribution of significantly enriched terms based on their functions on the basis of the first-round enrichment analyses of significantly differentially expressed genes with FC > 1.5 between SGR and PPR by Cytoscape and ClueGO (www.cytoscape.org). (d) Barrier-related significantly enriched terms revealed by Cytoscape and ClueGO between SGR and PPR in the second pathway analysis of significantly differentially expressed genes with FC > 1.5. (e) Representative barrier-related terms visualized by ClueGO. CASP, caspase; CDSN, corneodesmosin; FC, fold change; Nr., number; PPR, papulopustular rosacea; RNASeq, RNA sequencing; SGR, sebaceous gland−rich.
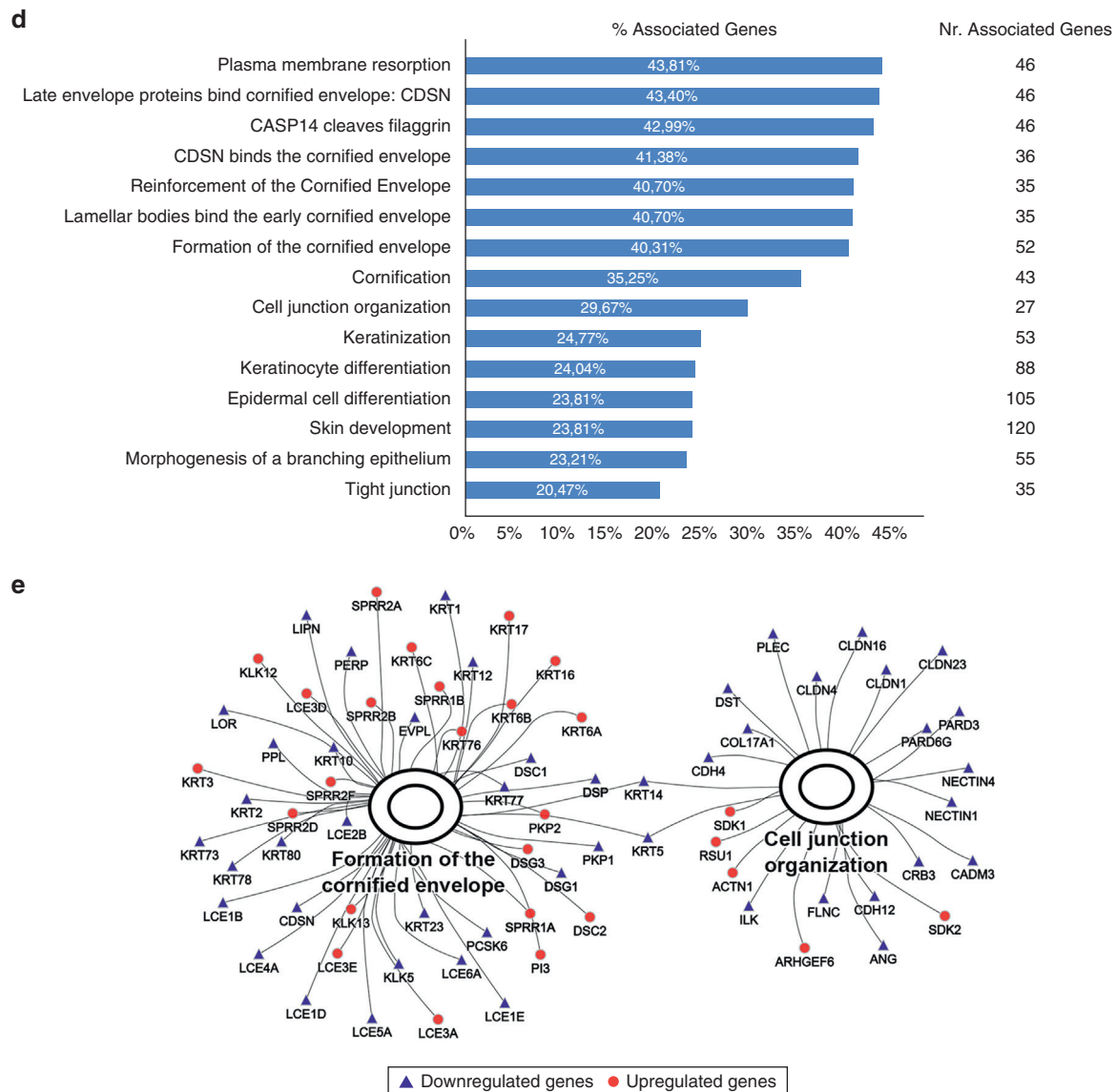
samples compared with SGR samples (Table 1, Supplementary Figure S1).

Next, we analyzed cornified envelope components at the protein level using IHC. LOR and KRT1 protein levels were significantly lower in PPR than SGR skin, whereas FLG levels were similar in the sample groups (Table 1, Figure 2). Among the previously mentioned enzymes, no significant differences in TGM5 were detected between healthy SGR and PPR samples (Table 1, Figure 2).

Intercellular lipid lamellae formation. Among molecules with a pivotal role in composing intercellular lipid lamellae, the gene expression level of *ABCA12* was assessed by RT-qPCR in PPR and SGR samples. According to our results,

ABCA12 was significantly downregulated in the diseased specimens (Table 1, Supplementary Figure S1).

Desmosome organization. The gene expression levels of desmosome components (*DSG1*, *DSC1*, *CDSN*, *PKP1*, and *CDH1*) were examined by RT-qPCR. We found that all investigated molecules were highly and significantly down-regulated in PPR specimens, except for *CDSN*. *CDSN* mRNA levels were not significantly different between the two groups (Table 1, Supplementary Figure S1). To validate our results at the protein level, we also examined two junction compo-nents, DSG1 and CDSN, by IHC. DSG1 protein levels were significantly lower in PPR compared with SGR samples, whereas CDSN protein was expressed at a similar level in the two sample groups (Table 1, Figure 2).

d

	% Associated Genes	Nr. Associated Genes
Plasma membrane resorption	43,81%	46
Late envelope proteins bind cornified envelope: CDSN	43,40%	46
CASP14 cleaves filaggrin	42,99%	46
CDSN binds the cornified envelope	41,38%	36
Reinforcement of the Cornified Envelope	40,70%	35
Lamellar bodies bind the early cornified envelope	40,70%	35
Formation of the cornified envelope	40,31%	52
Cornification	35,25%	43
Cell junction organization	29,67%	27
Keratinization	24,77%	53
Keratinocyte differentiation	24,04%	88
Epidermal cell differentiation	23,81%	105
Skin development	23,81%	120
Morphogenesis of a branching epithelium	23,21%	55
Tight junction	20,47%	35

e

▲ Downregulated genes   ● Upregulated genes

Figure 1. Continued

Corneocyte desquamation. We measured mRNA levels for skin barrier−related enzymes having a crucial role in desquamation (*KLK5*, *KLK7*, and *KLK14*). The expression levels for *KLK5*, *KLK7*, and *KLK14* were similar in PPR versus SGR samples (Table 1, Supplementary Figure S2). We immunostained for KLK5 in healthy SGR and PPR samples, and no significant differences between PPR and SGR were detected (Table 1, Figure 2).

Tight junction formation. The mRNA levels of tight junction components (*CLDN1*, *CLDN16*, *CLDN23*, and *OCLN*) were measured. The tight junction molecules were significantly downregulated in PPR samples compared with healthy SGR skin (Table 1, Supplementary Figure S2). To confirm our results at the protein level, we measured CLDN1 by IHC and detected significantly lower levels in PPR than SGR samples (Table 1, Figure 2).

Barrier alarmins. KRT6, KRT16, and KRT17 are highly induced in response to an epidermal barrier breach.

Therefore, we investigated the gene expression levels of these barrier alarmins. According to our results, the mRNA levels of *KRT6*, *KRT16*, and *KRT17* were significantly upregulated in PPR compared with SGR (Table 1, Supplementary Figure S2). Immunostaining of KRT6 confirmed our mRNA data. KRT6 was almost absent from SGR skin but highly expressed in PPR (Table 1, Figure 2).

AMPs. We also examined the gene expression levels for key components of the immunological barrier, including the following AMPs: S100A7, S100A8, S100A9, DEFB4B, LCN2, and cathelicidin. All of the investigated AMPs were significantly upregulated in PPR samples compared with healthy SGR skin samples (Table 1, Supplementary Figure S2). To confirm that the increased mRNA levels resulted in increased protein, we measured the protein levels of S100A8 and LCN2. S100A8 and LCN2 protein levels were significantly higher in PPR samples compared with controls (Table 1, Figure 2).

1942

Journal of Investigative Dermatology (2020), Volume 140

B Medgyesi et al.
Skin Barrier Alterations of PPR

Table 1. Comparison of Barrier Components in PPR and SGR Skin

Variable	RNASeq (PPR vs SGR)		qRT-PCR (PPR vs SGR)		IHC (PPR vs SGR)		ROS vs HC literature		AD vs HC literature	
	P-Value	FC	P-Value	FC[1]	P-Value	FC[1]	protein/mRNA data	(Ref.)	protein/mRNA data	(Ref.)
Cornified envelope formation										
FLG	NS		2.60E-03	2.95↓	NS		NS mRNA	(Deng et al., 2019)	↓ prot. and mRNA	(Brunello, 2018; De Benedetto et al., 2011; Ghosh et al., 2015; Pellerin et al., 2013; Sugiura et al., 2005)
KRT1	3.28E-03	2.86↓	<1.00E-4	2.20↓	4.80E-03	2.22↓	# ↓ prot. and mRNA		↓ prot. and mRNA	(Sugiura et al., 2005; Totsuka et al., 2017)
KRT10	3.28E-03	2.52↓	9.00E-04	2.75↓	Nd		NS mRNA	(Deng et al., 2019)		
LCE1D	2.32E-03	3.57↓	3.42E-02	1.97↓	Nd		# ↓ mRNA		↓ mRNA	(De Benedetto et al., 2011)
LCE1F	NS		NS		Nd		# NS mRNA			
LOR	8.65E-03	2.95↓	1.16E-02	2.03↓	2.11E-02	1.81↓	NS mRNA	(Deng et al., 2019)	↓ mRNA	(De Benedetto et al., 2011; Ghosh et al., 2015; Sugiura et al., 2005)
SPRR1A	1.17E-02	3.26↑	NS		Nd		# NS mRNA		↑ mRNA	(Sugiura et al., 2005)
SPRR2A	1.63E-03	8.64↑	2.59E-02	4.96↑	Nd		↑ mRNA		↑ mRNA	(De Benedetto et al., 2011; Sugiura et al., 2005)
TGM1	NS		NS		Nd		# NS mRNA		no available data	
TGM3	NS		NS		Nd		# NS mRNA		no available data	
TGM5	NS		NS		NS		# NS prot. and mRNA		no available data	
Intercellular lipid lamellae formation										
ABCA12B	NS		1.00E-03	2.09↓	Nd		# ↓ mRNA		no available data	
Corneodesmosome organization										
CDH1	3.57E-02	1.38↓	5.10E-03	1.60↓	Nd		# ↓ mRNA		no available data	
CDSN	3.57E-02	1.92↓	NS		NS		# NS mRNA		no available data	
DSC1	1.13E-03	2.49↓	1.50E-03	4.03↓	Nd		# ↓ mRNA		↓ prot.	(Totsuka et al., 2017)
DSG1	2.32E-03	1.85↓	<1.00E-4	5.76↓	1.60E-03	2.86↓	# ↓ prot. and mRNA			
PKP1	1.63E-03	2.79↓	5.00E-04	2.19↓	Nd		# ↓ mRNA		no available data	
Corneocyte desquamation										
KLK5	8.65E-03	1.69↓	NS		Nd		↑ exp. and act.	(Deng et al., 2019; Yamasaki and Gallo, 2011)	NS prot.	(Brunello, 2018; Rawlings and Voegeli, 2013)
KLK7	NS		NS		Nd		# NS mRNA		NS prot.	(Brunello, 2018; Igawa et al., 2017)
KLK14	NS		NS		Nd		# NS mRNA		NS prot. and mRNA	(Brunello, 2018; Rawlings and Voegeli, 2013)

(continued)

Table 1. Continued

| Variable	RNASeq (PPR vs SGR) P-Value	FC	qRT-PCR (PPR vs SGR) P-Value	FC[1]	IHC (PPR vs SGR) P-Value	FC[1]	ROS vs HC literature protein/mRNA data	(Ref.)	AD vs HC literature protein/mRNA data	(Ref.)
Tight junction formation										
CLDN1	**7.78E-04**	**2.22↓**	**1.30E-03**	**3.75↓**	**2.67E-02**	**1.91↓**	**↓ prot. and mRNA**	(Deng et al., 2019)	**↓ mRNA**	(De Benedetto et al., 2011)
CLDN16	**1.17E-02**	**1.68↓**	**<1.00E-4**	**3.44↓**	Nd		# **↓ mRNA**		NS mRNA	
CLDN23	**1.13E-03**	**3.28↓**	**1.26E-02**	**2.56↓**	Nd		# **↓ mRNA**		**↓ mRNA**	
OCLN	NS		**<1.00E-4**	**3.04↓**	Nd		# **↓ mRNA**		NS prot. and mRNA	
Barrier alarmins										
KRT6A	**4.57E-03**	**5.03↑**	**3.70E-03**	**4.92↑**	**1.00E-03**	**109.28↑**	# **↑ prot. and mRNA**		**↑ mRNA**	(Ghosh et al., 2015; Sugiura et al., 2005)
KRT16	**1.57E-02**	**2.50↑**	**6.00E-04**	**9.76↑**	Nd		# **↑ mRNA**		**↑ mRNA**	
KRT17	**8.65E-03**	**4.16↑**	**1.28E-02**	**3.26↑**	Nd		# **↑ mRNA**		**↑ mRNA**	(Sugiura et al., 2005)
AMPs										
DEFB4B	**7.78E-04**	**84.35↑**	**3.82E-02**	**62.35↑**	Nd		# **↑ mRNA**		NS mRNA	(Sugiura et al., 2005)
CAMP	**4.58E-02**	**2.91↑**	**3.44E-02**	**7.90↑**	Nd		**↑ prot. and mRNA**	(Yamasaki et al., 2007)	controversial	(Ballardini et al., 2009; Gambichler et al., 2008; Patra et al., 2018)
LCN2	**3.28E-03**	**6.93↑**	**3.15E-02**	**3.46↑**	**4.60E-03**	**3.08↑**	# **↑ prot. and mRNA**		no available data	
S100A7	**1.13E-03**	**19.30↑**	**< 1.00E-4**	**19.68↑**	Nd		# **↑ mRNA**		**↑ mRNA**	(De Benedetto et al., 2011; Sugiura et al., 2005)
S100A8	**7.78E-04**	**24.75↑**	**2.00E-04**	**21.75↑**	**4.54E-02**	**2.20↑**	# **↑ prot. and mRNA**		**↑ mRNA**	
S100A9	**7.78E-04**	**29.64↑**	**7.00E-04**	**18.57↑**	Nd		# **↑ mRNA**		**↑ mRNA**	

Abbreviations: act., activity; AD, atopic dermatitis; CAMP, cathelicidin; CDSN, corneodesmosin; DSG1, desmoglein 1; exp., expression; FC, fold change; HC, healthy control; IHC, immunohistochemistry; KLK, kallikrein; nd, not determined; NS, not significant; PPR, papulopustular rosacea; prot., protein; Ref., reference; RNASeq, RNA sequencing; ROS, rosacea; SGR, sebaceous gland–rich.

Boxes represent the studied seven major groups of barrier composing molecules. The first column contains the molecules that have been investigated in our study. The second, third, and fourth columns summarize our findings according to the applied methods: RNASeq, qRT-PCR and IHC, respectively. Eight samples were examined in each group regarding all the investigated molecules.

Available literature data about papulopustular rosacea regarding all the investigated molecules, as well as our present findings from column 1−3 are compiled in Column 5. In this column, # represents that to our knowledge our study provides novel, previously unreported data, whereas the absence of # represents preexisting literature data. Available literature data about atopic dermatitis regarding all the investigated molecules are referenced in column 6. Comparison of column 5 and 6 highlights the similarities between the barrier alterations of these two skin disorders.

Statistical analyses between protein and mRNA levels were determined by two-sample *t*-test. Bold type indicates data with significant differences.

[1]Arrows indicate the direction of significant changes.
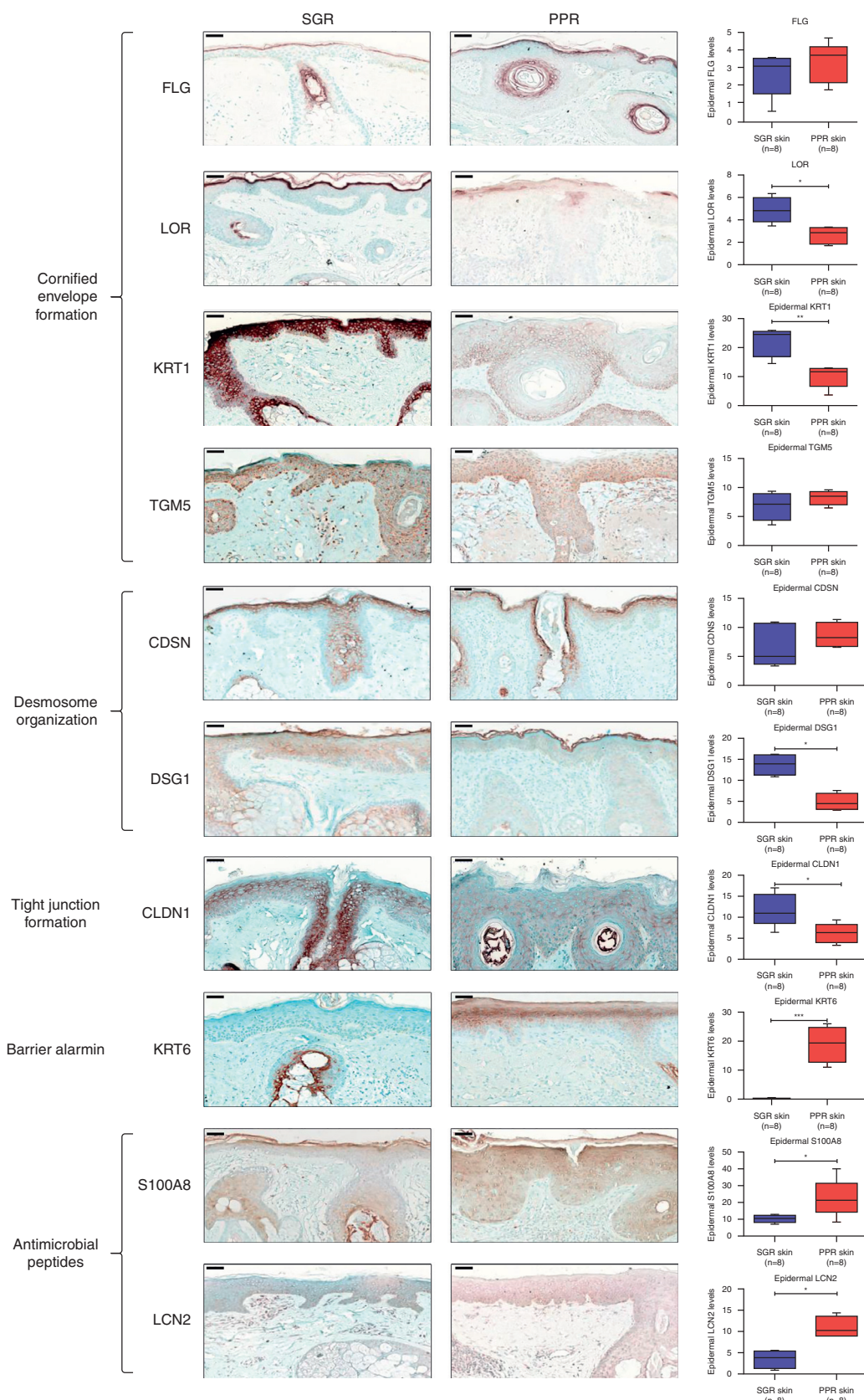
Figure 2. Prominent differences in the protein expression levels of skin barrier–related molecules between PPR and healthy SGR skin samples. Representative images for immunostaining and quantification of epidermal levels of FLG, LOR, KRT1, TGM5, CDSN, DSG1, CLDN1, KRT6, S100A8, and LCN2 in SGR and PPR skin sections. The graphs show the mean ± 95% confidence interval of measured protein levels (*$P < 0.05$; **$P < 0.01$; ***$P < 0.001$, as determined by two-sample t-test). CDSN, corneodesmosin; DSG1, desmoglein 1; PPR, papulopustular rosacea; SGR, sebaceous gland–rich. Bar = 50 μm.
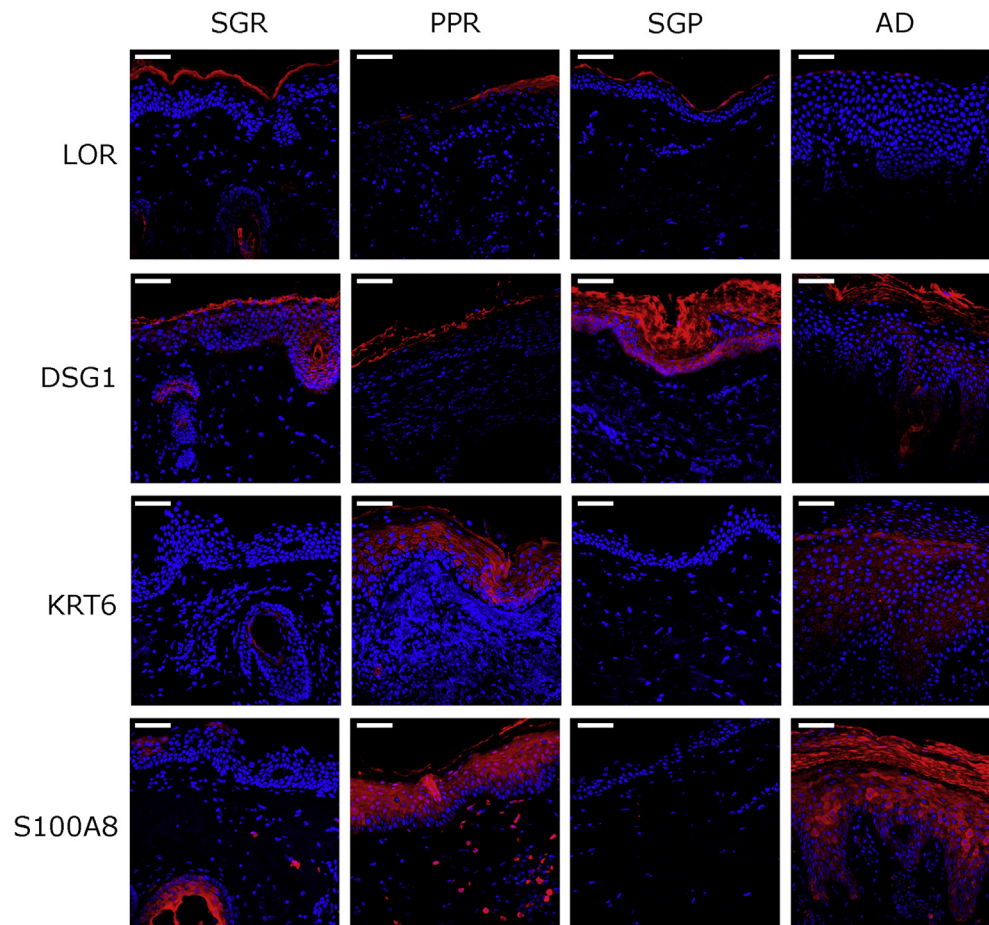
Figure 3. Highly similar barrier alteration occurs in PPR and AD. PPR and AD, as well as their respective control samples (SGR and SGP), were immunostained. Representative images for immunofluorescent staining of epidermal levels of LOR, DSG1, KRT6, and S100A8 in SGR, PPR, SGP, and AD skin sections. AD, atopic dermatitis; DSG1, desmoglein1; PPR, papulopustular rosacea; SGP, sebaceous gland—poor; SGR, sebaceous gland—rich. Bar = 50 μm.

Disrupted skin barrier features of PPR are similar to that of AD

Literature search. As barrier alterations in PPR seemed to be similar to that of lesional AD skin, we reviewed the literature on AD barrier damage and compared barrier alterations of the two disorders (Table 1). According to the literature search, the skin barrier alterations were similar in PPR and AD skin compared with the respective healthy control skin (SGR and sebaceous gland—poor [SGP]).

Immunofluorescent staining. To confirm similarities in skin barrier changes between PPR and AD, immunofluorescent staining was performed in PPR and AD samples and the respective SGR and SGP skin specimens. According to the immunostaining results, a cornified envelope structural molecule (LOR) and key components of desmosomes (DSG1) and tight junctions (CLDN1) were highly downregulated in PPR and AD samples compared with controls (Figure 3). In contrast, the barrier alarmin KRT6 and the AMP S100A8 were almost absent from healthy skin types and were expressed at high levels in PPR and AD skin specimens (Figure 3). Notably, the expression patterns of these proteins were similar in PPR and AD skin (Figure 3).

DISCUSSION
Clinical features and functional studies on the affected facial skin of patients with rosacea indicate the presence of permeability barrier alterations (Darlenski et al., 2013; Powell and Ni Raghallaigh, 2011). However, no detailed analysis of skin barrier disruption in rosacea at the molecular level has been conducted so far. In the present study, we performed whole transcriptomic analysis (RNASeq) of PPR skin samples, and gene expression profiles of diseased skin were compared with that of healthy SGR skin. According to our findings, all major components of the skin barrier are severely altered in PPR.

An intact skin barrier is essential for maintaining homeostasis as it protects the body against external agents and microbes and provides a waterproof cover. According to the literature, stratum corneum, the outermost layer of the epidermis, and tight junctions are considered the most important components of the skin permeability barrier (Egawa and Kabashima, 2016; Egawa and Kabashima, 2018). Molecules forming the stratum corneum can be further divided into four groups: cornified envelope formation, intercellular lipid lamellae formation, corneodesmosome organization, and corneocyte desquamation (Egawa and Kabashima, 2016; Egawa and Kabashima, 2018).

Cornified envelope is built up from several types of intracellular structure proteins, including FLG, LOR, LCE, and SPRR proteins; envoplakin; periplakin; involucrin; and KRT filaments that are derived from keratohyalin granules (Carregaro et al., 2013; Egawa and Kabashima, 2016; Koch et al., 2000; Palmer et al., 2006). These proteins undergo

cross-linking, which is catalyzed by TGM1, TGM3, and TGM5 (Eckert et al., 2005). According to our results, FLG, LOR, KRT1, KRT10, and LCE1D were significantly downregulated, whereas SPRR2A was significantly upregulated in PPR skin compared with healthy SGR skin. The significant decrease in LOR and KRT1 levels was also confirmed at the protein level. Regarding the expression of TGMs, no significant difference was detected either at mRNA or protein levels.

Lipid lamellae formation is also a critical event in the development of intact stratum corneum, in which lipoxygenases (ALOX12B and ALOXB3) and lipid transporters (ABCA12) are essential to lipid synthesis and transport (Iwai et al., 2012; Kelsell et al., 2005; Krieg and Fürstenberger, 2014). In our study, *ABCA12* was significantly downregulated at the mRNA level in PPR compared with controls.

Another component of the stratum corneum is the desmosome apparatus, which is responsible for cell adhesion of corneocytes (Egawa and Kabashima, 2016; Egawa and Kabashima, 2018). Based on our findings, desmosomes are highly disrupted in PPR, as demonstrated by the significantly decreased gene expression levels of *CDH1*, *CDSN*, *DSC1*, *DSG1*, and *PKP1*. The significant decrease in DSG1 was also confirmed at the protein level by IHC.

In the stratum corneum, corneocytes are shed as part of an event called desquamation, which is primarily regulated by KLKs (KLK5, KLK7, and KLK14) via a pH-dependent proteolytic cascade (Brattsand et al., 2005; Rippke et al., 2004). In this study, we detected similar gene expression levels of *KLK5*, *KLK7*, and *KLK14* in lesional PPR compared with healthy skin; however, the enzymes' protein levels and activity were not examined.

In addition to the stratum corneum, tight junctions are also key components for the integrity of the skin barrier by sealing adjacent keratinocytes in the stratum granulosum and acting as a barrier for water and solutes. Tight junctions are composed of transmembrane proteins, particularly the CLDNs and OCLN (Kirschner et al., 2010; Yokouchi et al., 2015). In our study, mRNA levels for *CLDN1*, *CLDN16*, *CLDN23*, and *OCLN* were significantly decreased in PPR compared with controls. The significant decrease in CLDN1 was confirmed at the protein level by IHC.
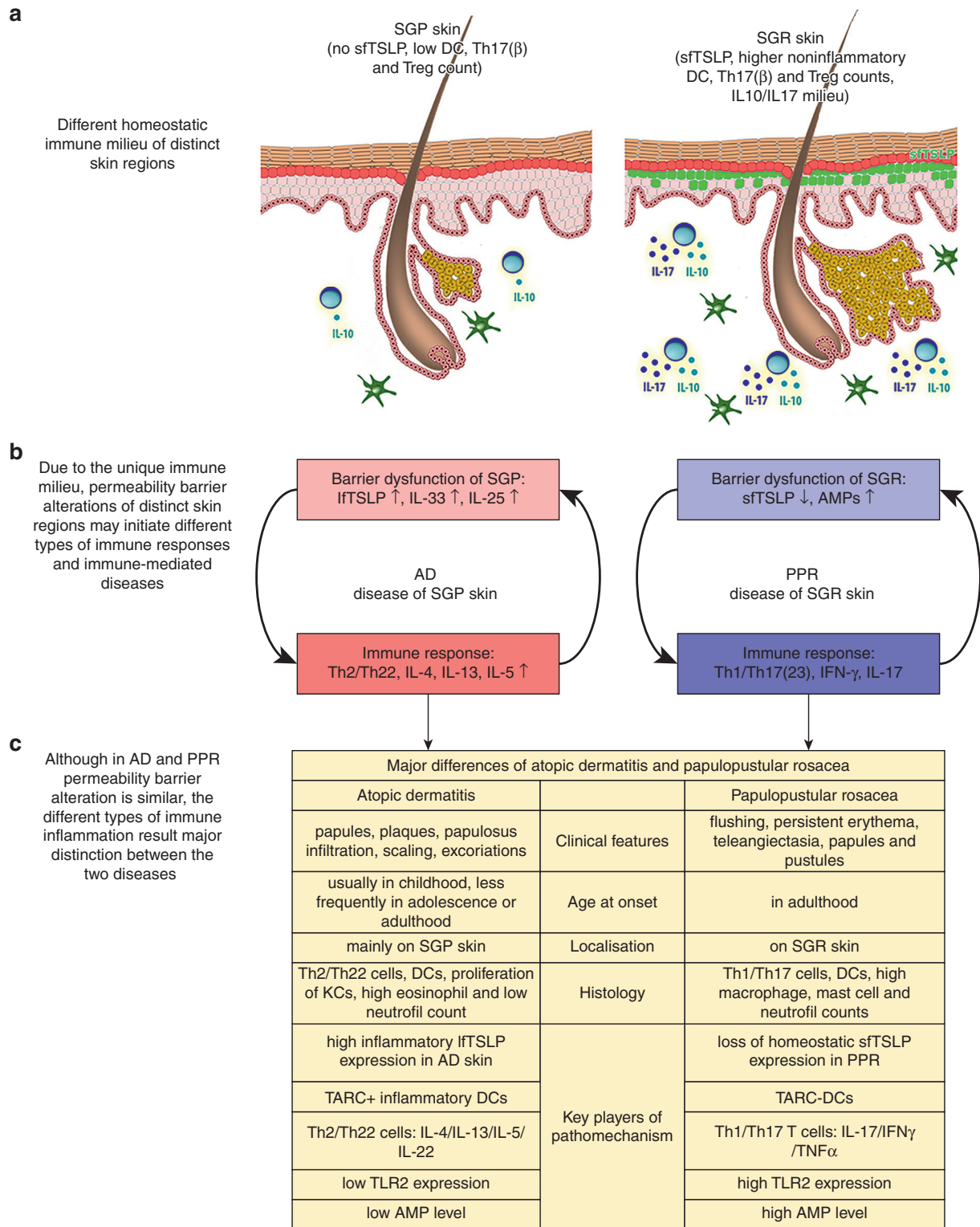
In parallel with the stratum corneum and tight junction components, we focused on investigating two additional groups of molecules, key barrier alarmins and AMPs, because the expression levels of these molecules are tightly connected with the level of permeability barrier structural components (Borkowski and Gallo, 2011; Zhang et al., 2019). In our study, all investigated barrier alarmins (KRT6A, KRT16, and KRT17) and AMPs (cathelicidin, hBD-2, LCN2, S100A7, S100A8, and S100A9) were significantly upregulated in PPR skin compared with controls. The significantly higher presence of LCN2, S100A8, and KRT6 in PPR was confirmed at the protein level.

To our knowledge, until now, only one study has investigated rosacea samples at a whole transcriptomic level. In this previous study, the authors focused on examining the immunological characteristics of different rosacea subtypes, and no data were published on barrier components (Buhl et al., 2015). Another study, performed by Deng et al.,

focused on mRNA expression levels of cornified envelope components, including *KRT10*, *FLG*, and *LOR* in different rosacea subtypes (Deng et al., 2019). They also studied the tight junction protein CLDN1 and could detect significantly lower gene expression and protein levels of CLDN1 in PPR samples compared with controls, in agreement with our results. Regarding the mRNA levels of *KRT10* and *LOR*, the authors of this study did not find significant differences when comparing PPR to controls, and protein levels were not assessed (Deng et al., 2019). The expression of KLK5 in rosacea has been studied previously by another workgroup, and its mRNA and protein levels were demonstrated to be significantly increased, in parallel with elevated enzyme activity; however, the authors did not specify which rosacea subtype had been assessed (Morizane et al., 2010; Yamasaki and Gallo, 2011). In our study, in PPR, we could not detect significantly elevated *KLK5* mRNA levels, but protein levels and enzyme activity were not assessed. Among AMPs, only the expression of cathelicidin was assessed previously in PPR, whereas data regarding hBD-2 is available only in ocular rosacea (Gökçnar et al., 2019; Morizane et al., 2010; Yamasaki and Gallo, 2011). In line with these previous results, in our study, cathelicidin and hBD-2 were significantly upregulated in PPR as compared with SGP skin at the mRNA level.

As a whole, our in-depth molecular biological investigation, using whole transcriptomic and bioinformatics analyses, qRT-PCR, and quantitative IHC, indicate that all major components of the permeability skin barrier are severely disrupted in PPR, which may significantly contribute to disease pathophysiology. Barrier alterations have gained far-reaching importance in recent years. In AD, it has been proven that barrier disruption is able to induce skin inflammation, and, in this manner, can be considered as an initiator of disease pathogenesis. From this point of view, it is quite interesting that we could detect highly similar barrier alterations in PPR and AD. According to our literature search and results, these similarities included the altered expression of cornified envelope components, desmosome and tight junction molecules, barrier alarmins, and AMPs. Moreover, we could confirm some of these similarities at the protein level by immunofluorescent staining of selected molecules. The demonstrated similarity between the barrier disruptions in PPR and AD is surprising because, up until now, mainly the differences in clinical features and immune composition of these diseases have been highlighted (Figure 4).

Although it is well known that barrier dysfunction is a potent initiator of inflammation in AD, on the basis of our results, we cannot determine the role of barrier alterations in rosacea, if it is the result or the cause of inflammation. Barrier damage may occur because of the Th1/Th17 type inflammation that is characteristic in rosacea, and IL-17A recently has been shown to downregulate *FLG*, *LOR*, and *KRT10* mRNA levels in organotypic three-dimensional skin equivalents (Pfaff et al., 2017). In contrast, it is also possible that dysfunctional barrier is the initiating factor of rosacea development. Although barrier alteration is an adjuvant factor for Th2 type inflammation in AD, the reason why similar barrier disruption may precipitate Th1/Th17 type inflammation in rosacea could be that AD has an SGP region

a

Different homeostatic immune milieu of distinct skin regions

SGP skin
(no sfTSLP, low DC, Th17(β) and Treg count)

SGR skin
(sfTSLP, higher noninflammatory DC, Th17(β) and Treg counts, IL10/IL17 milieu)

b

Due to the unique immune milieu, permeability barrier alterations of distinct skin regions may initiate different types of immune responses and immune-mediated diseases

Barrier dysfunction of SGP:
lfTSLP ↑, IL-33 ↑, IL-25 ↑

AD
disease of SGP skin

Immune response:
Th2/Th22, IL-4, IL-13, IL-5 ↑

Barrier dysfunction of SGR:
sfTSLP ↓, AMPs ↑

PPR
disease of SGR skin

Immune response:
Th1/Th17(23), IFN-γ, IL-17

c

Although in AD and PPR permeability barrier alteration is similar, the different types of immune inflammation result major distinction between the two diseases

Major differences of atopic dermatitis and papulopustular rosacea		
Atopic dermatitis		Papulopustular rosacea
papules, plaques, papulosus infiltration, scaling, excoriations	Clinical features	flushing, persistent erythema, teleangiectasia, papules and pustules
usually in childhood, less frequently in adolescence or adulthood	Age at onset	in adulthood
mainly on SGP skin	Localisation	on SGR skin
Th2/Th22 cells, DCs, proliferation of KCs, high eosinophil and low neutrofil count	Histology	Th1/Th17 cells, DCs, high macrophage, mast cell and neutrofil counts
high inflammatory lfTSLP expression in AD skin	Key players of pathomechanism	loss of homeostatic sfTSLP expression in PPR
TARC+ inflammatory DCs		TARC-DCs
Th2/Th22 cells: IL-4/IL-13/IL-5/IL-22		Th1/Th17 T cells: IL-17/IFNγ/TNFα
low TLR2 expression		high TLR2 expression
low AMP level		high AMP level

Figure 4. The possible role of permeability barrier alteration in the pathogenesis of PPR. Until now, when comparing AD and PPR, mainly the differences in their clinical and immunological characteristics were pronounced by dermatologists. However, based on our results, these two skin disorders can be considered from another point of view, because both are characterized by severe and notably similar skin barrier damage, although being developed on distinct skin areas. We propose that the prominently different steady-state immune and barrier features of (**a**) the skin regions (SGR and SGP skin) where these diseases prefer to localize can influence (**b**) the barrier damage—connected inflammation differently, leading to (**c**) region-specific immune-mediated skin diseases and explaining the prominent distinctions between AD and PPR. AD, atopic dermatitis; AMP, antimicrobial peptide; DC, dendritic cell; KC, keratinocyte; lfTSLP, long form thymic stromal lymphopoietin; sfTSLP, short form thymic stromal lymphopoietin; PPR, papulopustular rosacea; SGP, sebaceous gland—poor; SGR, sebaceous gland—rich; Th, T helper; Th17(β), noninflammatory Th17 cell; Th17(23), inflammatory Th17 cell; TLR2, toll-like receptor 2; Treg, regulatory T cell.

preference, whereas rosacea localizes exclusively on SGR skin. SGR and SGP skin areas have prominently different homeostatic immune and barrier characteristics (Béke et al., 2018; Dajnoki et al., 2017). Whereas SGR skin regions dispose significantly higher AMP levels, noninflammatory Th17(β) and regulatory T-cell counts, and constitutive expression of homeostatic short form thymic stromal lymphopoietin (sfTSLP), SGP skin is characterized by low AMP levels and T-cell counts, without TSLP presence under steady-state (Béke et al., 2018; Dajnoki et al., 2017). These features of the skin seem to be very similar to that of another barrier, namely the gut, where the regional immune-related differences are well known. Th17(β) cells are enriched and sfTSLP is expressed in the small intestine, in contrast to the colon, where Th17(β) cells are absent and sfTSLP is present only in the proximal part (Iliev et al., 2009; Rimoldi et al., 2005). It has been raised that these unique immune and barrier characteristics of different gut sections can lead to distinct types of immune-mediated diseases. In Crohn's disease, the loss of sfTSLP from the small intestine can promote the activation of inflammatory Th1/Th17 cells (Iliev et al., 2009; Rimoldi et al., 2005), whereas in ulcerative colitis, significantly increased inflammatory long form TSLP levels initiate Th2 type inflammation in the colon (Fornasa et al., 2015). On the basis of these findings, we hypothesize that similar barrier alterations of SGR and SGP skin regions, because of their different homeostatic immune and barrier milieu, initiate distinct immune-mediated skin diseases with unique clinical features driven by different Th subsets (AD on SGP and PPR on SGR areas) (Figure 4). Notably, De Benedetto et al. already raised the possibility that barrier defects can lead to the production of keratinocyte-derived mediators including pro-Th2 and pro-Th17 types that affect the characteristics of Th response (De Benedetto et al., 2012).

To determine if PPR barrier damage is the initiator of the disease or a consequence of manifested inflammation, the exact time of barrier disruption should be studied and a detailed analysis of the perilesional and/or nonlesional skin of patients with PPR should be performed in the future. Moreover, analogous experiments are needed in other subtypes of rosacea.

In summary, our results unambiguously prove the presence of severe barrier alterations in the facial skin of patients with PPR; thus, we suggest that skin barrier restoring therapies should be incorporated into clinical guidelines for rosacea management, similar to that of AD.

MATERIALS AND METHODS

Skin biopsies
Skin punch biopsies (0.5–1 cm^2) were taken from normal SGR skin sites of eight healthy individuals (mean age ± SD: 56.25 ± 13.11 years) undergoing plastic surgery and from lesional skin of eight patients with PPR (mean age ± SD: 59.38 ± 13.59 years) (Supplementary Table S4). Written informed consent according to the Declaration of Helsinki principles was obtained by all individuals before participating in the study. The study was approved by the local ethics committee of the University of Debrecen.

RNA isolation and reverse transcription
Samples were homogenized in Tri reagent (Sigma-Aldrich, St. Louis, MO) with Tissue Lyser (Qiagen, Hilden, Germany) using previously autoclaved metal beads (Qiagen). RNA concentration and purity were measured and cDNA was synthesized using the High Capacity cDNA Archive Kit (Invitrogen, Thermo Fisher Scientific, Waltham, MA).

RT-qPCR
RT-PCR was carried out in triplicate using pre-designed MGB assays (Thermo Fisher Scientific). The assessed TaqMan Gene Expression assays are listed in Supplementary Materials and Methods. All reactions were performed with an ABI PRISM 7000 Sequence Detection System. Relative mRNA levels were calculated using the 2-ΔΔCt method normalized to the expression of PPIA mRNA.

RNASeq analysis
Complementary DNA library for RNASeq was generated from 1 μg total RNA using TruSeq RNA Sample Preparation Kit (Illumina, San Diego, CA) according to the manufacturer's protocol. A single read 50 base pair sequencing run was performed on Illumina HiScan SQ instrument (Illumina), and 16–18 million reads per sample were obtained. Sequenced reads were aligned to Human Genome v19 using TopHat and Cufflinks algorithms and bam files were generated. StrandNGS software was used for further statistical analysis. To identify statistically significant gene expression patterns, nonparametric Wilcoxon–Mann–Whitney test was used. Library preparations, sequencing, and data analysis were performed at the Genomic Medicine and Bioinformatics Core Facility of University of Debrecen. RNA sequencing data of our samples were deposited to the Sequence Read Archive database (https://www.ncbi.nlm.nih.gov/sra), under accession numbers PRJNA421246 and PRJNA592080.

Pathway analyses
Multiple bioinformatics analyses were performed by Cytoscape ClueGO bioinformatics tool. Pathway enrichment analyses were performed on all DEGs with fold change ≥ 1.5. The details of our analytical approach can be found in the Supplementary Materials and Methods.

Immunohistochemistry
For IHC analyses, paraffin-embedded sections from patients and healthy controls were deparaffinized. Heat-induced antigen retrieval was performed. Sections were stained with primary antibodies listed in Supplementary Materials and Methods. Subsequently, anti-mouse/rabbit horseradish peroxidase—conjugated secondary antibody (Biogenex, Fremont, CA) was employed. Staining was detected with the Vector NovaRed Kit (Vector Laboratories, Burlingame, CA). Sections were counterstained with methylene green and digitized by Whole Slide Imaging, and Pannoramic Viewer software was used for the evaluation of the degree of staining of the slides.

Statistical analysis
Data distribution was analyzed by Kolmogorov-Smirnov test. Because our data showed normal distribution, two groups of samples were compared statistically by two-sample t-test. Differences between the groups were demonstrated using mean ± 95% confidence interval. P-values < 0.05 were considered statistically significant (*$P < 0.05$; **$P < 0.01$; ***$P < 0.001$). Statistical data was analyzed using GraphPad Prism v6 (GraphPad Software Inc., La Jolla, CA) and SPSS 25 (SPSS package for Windows, Chicago, IL).

Additional details are provided in the Supplementary Information online.

Data availability statement
The data that support the findings of this study are available from the corresponding author upon reasonable request.

ORCIDs

Barbara Medgyesi: https://orcid.org/0000-0001-8800-7693
Zsolt Dajnoki: https://orcid.org/0000-0002-7787-1002
Gabriella Béke: https://orcid.org/0000-0003-3113-2287
Krisztián Gáspár: https://orcid.org/0000-0001-6530-7052
Imre Lőrinc Szabó: https://orcid.org/0000-0002-9628-4372
Eszter Anna Janka: https://orcid.org/0000-0003-0724-5281
Szilárd Póliska: https://orcid.org/0000-0002-9722-251X
Zoltán Hendrik: https://orcid.org/0000-0001-8546-2148
Gábor Méhes: https://orcid.org/0000-0003-2503-7451
Dániel Törőcsik: https://orcid.org/0000-0002-6094-6266
Tamás Bíró: https://orcid.org/0000-0002-3770-6221
Anikó Kapitány: https://orcid.org/0000-0003-4540-5258
Andrea Szegedi: https://orcid.org/0000-0003-2109-9014

SUPPLEMENTARY MATERIAL

Supplementary material is linked to the online version of the paper at www.jidonline.org, and at https://doi.org/10.1016/j.jid.2020.02.025.

REFERENCES

Ballardini N, Johansson C, Lilja G, Lindh M, Linde Y, Scheynius A, et al. Enhanced expression of the antimicrobial peptide LL-37 in lesional skin of adults with atopic eczema. Br J Dermatol 2009;161:40–7.

Béke G, Dajnoki Z, Kapitány A, Gáspár K, Medgyesi B, Póliska S, et al. Immunotopographical differences of human skin. Front Immunol 2018;9:424.

Bindea G, Mlecnik B, Hackl H, Charoentong P, Tosolini M, Kirilovsky A, et al. ClueGO: a Cytoscape plug-in to decipher functionally grouped gene ontology and pathway annotation networks. Bioinformatics 2009;25:1091–3.

Borkowski AW, Gallo RL. The coordinated response of the physical and antimicrobial peptide barriers of the skin. J Invest Dermatol 2011;131:285–7.

Brattsand M, Stefansson K, Lundh C, Haasum Y, Egelrud T. A proteolytic cascade of kallikreins in the stratum corneum. J Invest Dermatol 2005;124:198–203.

Brunello L. Atopic dermatitis. Nat Rev Dis Primers 2018;4:2.

Buechner SA. Rosacea: an update. Dermatology 2005;210:100–8.

Buhl T, Sulk M, Nowak P, Buddenkotte J, McDonald I, Aubert J, et al. Molecular and morphological characterization of inflammatory infiltrate in rosacea reveals activation of Th1/Th17 pathways. J Invest Dermatol 2015;135:2198–208.

Carregaro F, Stefanini AC, Henrique T, Tajara EH. Study of small proline-rich proteins (SPRRs) in health and disease: a review of the literature. Arch Dermatol Res 2013;305:857–66.

Crawford GH, Pelle MT, James WD. Rosacea: I. Etiology, pathogenesis, and subtype classification. J Am Acad Dermatol 2004;51:327–41:quiz 42–4.

Dajnoki Z, Béke G, Kapitány A, Mócsai G, Gáspár K, Rühl R, et al. Sebaceous gland-rich skin is characterized by TSLP expression and distinct immune surveillance which is disturbed in rosacea. J Invest Dermatol 2017;137:1114–25.

Darlenski R, Kazandjieva J, Tsankov N, Fluhr JW. Acute irritant threshold correlates with barrier function, skin hydration and contact hypersensitivity in atopic dermatitis and rosacea. Exp Dermatol 2013;22:752–3.

De Benedetto A, Kubo A, Beck LA. Skin barrier disruption: a requirement for allergen sensitization? J Invest Dermatol 2012;132:949–63.

De Benedetto A, Rafaels NM, McGirt LY, Ivanov AI, Georas SN, Cheadle C, et al. Tight junction defects in patients with atopic dermatitis. J Allergy Clin Immunol 2011;127:773–86.e1–7.

Deng Z, Chen M, Xie H, Jian D, Xu S, Peng Q, et al. Claudin reduction may relate to an impaired skin barrier in rosacea. J Dermatol 2019;46:314–21.

Eckert RL, Sturniolo MT, Broome AM, Ruse M, Rorke EA. Transglutaminase function in epidermis. J Invest Dermatol 2005;124:481–92.

Egawa G, Kabashima K. Multifactorial skin barrier deficiency and atopic dermatitis: essential topics to prevent the atopic march. J Allergy Clin Immunol 2016;138:350–8.e1.

Egawa G, Kabashima K. Barrier dysfunction in the skin allergy. Allergol Int 2018;67:3–11.

Fornasa G, Tsilingiri K, Caprioli F, Botti F, Mapelli M, Meller S, et al. Dichotomy of short and long thymic stromal lymphopoietin isoforms in inflammatory disorders of the bowel and skin. J Allergy Clin Immunol 2015;136:413–22.

Gallo RL, Granstein RD, Kang S, Mannis M, Steinhoff M, Tan J, et al. Rosacea comorbidities and future research: the 2017 update by the National Rosacea Society Expert Committee. J Am Acad Dermatol 2018a;78:167–70.

Gallo RL, Granstein RD, Kang S, Mannis M, Steinhoff M, Tan J, et al. Standard classification and pathophysiology of rosacea: the 2017 update by the National Rosacea Society Expert Committee. J Am Acad Dermatol 2018b;78:148–55.

Gambichler T, Skrygan M, Tomi NS, Othlinghaus N, Brockmeyer NH, Altmeyer P, et al. Differential mRNA expression of antimicrobial peptides and proteins in atopic dermatitis as compared to psoriasis vulgaris and healthy skin. Int Arch Allergy Immunol 2008;147:17–24.

Ghosh D, Ding L, Sivaprasad U, Geh E, Biagini Myers J, Bernstein JA, et al. Multiple transcriptome data analysis reveals biologically relevant atopic dermatitis signature genes and pathways. PLOS ONE 2015;10:e0144316.

Gökçnar NB, Karabulut AA, Onaran Z, Yumuşak E, Budak Yldran FA. Elevated tear human neutrophil peptides 1–3, human beta defensin-2 levels and conjunctival cathelicidin LL-37 gene expression in ocular rosacea. Ocul Immunol Inflamm 2019;27:1174–83.

Igawa S, Kishibe M, Minami-Hori M, Honma M, Tsujimura H, Ishikawa J, et al. Incomplete KLK7 secretion and upregulated LEKTI expression underlie hyperkeratotic stratum corneum in atopic dermatitis. J Invest Dermatol 2017;137:449–56.

Iliev ID, Spadoni I, Mileti E, Matteoli G, Sonzogni A, Sampietro GM, et al. Human intestinal epithelial cells promote the differentiation of tolerogenic dendritic cells. Gut 2009;58:1481–9.

Iwai I, Han H, den Hollander L, Svensson S, Ofverstedt LG, Anwar J, et al. The human skin barrier is organized as stacked bilayers of fully extended ceramides with cholesterol molecules associated with the ceramide sphingoid moiety. J Invest Dermatol 2012;132:2215–25.

Jenei A, Dajnoki Z, Medgyesi B, Gáspár K, Béke G, Kinyó Á, et al. Apocrine gland-rich skin has a non-inflammatory IL-17-related immune milieu, that turns to inflammatory IL-17-mediated disease in hidradenitis suppurativa. J Invest Dermatol 2019;139:964–8.

Kelsell DP, Norgett EE, Unsworth H, Teh MT, Cullup T, Mein CA, et al. Mutations in ABCA12 underlie the severe congenital skin disease harlequin ichthyosis. Am J Hum Genet 2005;76:794–803.

Kirschner N, Houdek P, Fromm M, Moll I, Brandner JM. Tight junctions form a barrier in human epidermis. Eur J Cell Biol 2010;89:839–42.

Koch PJ, de Viragh PA, Scharer E, Bundman D, Longley MA, Bickenbach J, et al. Lessons from loricrin-deficient mice: compensatory mechanisms maintaining skin barrier function in the absence of a major cornified envelope protein. J Cell Biol 2000;151:389–400.

Krieg P, Fürstenberger G. The role of lipoxygenases in epidermis. Biochim Biophys Acta 2014;1841:390–400.

Morizane S, Yamasaki K, Kabigting FD, Gallo RL. Kallikrein expression and cathelicidin processing are independently controlled in keratinocytes by calcium, vitamin D(3), and retinoic acid. J Invest Dermatol 2010;130:1297–306.

Palmer CN, Irvine AD, Terron-Kwiatkowski A, Zhao Y, Liao H, Lee SP, et al. Common loss-of-function variants of the epidermal barrier protein filaggrin

are a major predisposing factor for atopic dermatitis. Nat Genet 2006;38: 441−6.

Patra V, Mayer G, Gruber-Wackernagel A, Horn M, Lembo S, Wolf P. Unique profile of antimicrobial peptide expression in polymorphic light eruption lesions compared to healthy skin, atopic dermatitis, and psoriasis. Photodermatol Photoimmunol Photomed 2018;34:137−44.

Pellerin L, Henry J, Hsu CY, Balica S, Jean-Decoster C, Méchin MC, et al. Defects of filaggrin-like proteins in both lesional and nonlesional atopic skin. J Allergy Clin Immunol 2013;131:1094−102.

Pfaff CM, Marquardt Y, Fietkau K, Baron JM, Lüscher B. The psoriasis-associated IL-17A induces and cooperates with IL-36 cytokines to control keratinocyte differentiation and function. Sci Rep 2017;7:15631.

Powell FC, Ni Raghallaigh S. Interventions for 'rosacea'. Br J Dermatol 2011;165:707−8.

Rawlings AV, Voegeli R. Stratum corneum proteases and dry skin conditions. Cell Tissue Res 2013;351:217−35.

Rimoldi M, Chieppa M, Salucci V, Avogadri F, Sonzogni A, Sampietro GM, et al. Intestinal immune homeostasis is regulated by the crosstalk between epithelial cells and dendritic cells. Nat Immunol 2005;6:507−14.

Rippke F, Schreiner V, Doering T, Maibach HI. Stratum corneum pH in atopic dermatitis: impact on skin barrier function and colonization with *Staphylococcus aureus*. Am J Clin Dermatol 2004;5:217−23.

Steinhoff M, Buddenkotte J, Aubert J, Sulk M, Novak P, Schwab VD, et al. Clinical, cellular, and molecular aspects in the pathophysiology of rosacea. J Investig Dermatol Symp Proc 2011;15:2−11.

Sugiura H, Ebise H, Tazawa T, Tanaka K, Sugiura Y, Uehara M, et al. Large-scale DNA microarray analysis of atopic skin lesions shows overexpression of an epidermal differentiation gene cluster in the alternative pathway and lack of protective gene expression in the cornified envelope. Br J Dermatol 2005;152:146−9.

Totsuka A, Omori-Miyake M, Kawashima M, Yagi J, Tsunemi Y. Expression of keratin 1, keratin 10, desmoglein 1 and desmocollin 1 in the epidermis: possible downregulation by interleukin-4 and interleukin-13 in atopic dermatitis. Eur J Dermatol 2017;27:247−53.

Yamasaki K, Di Nardo A, Bardan A, Murakami M, Ohtake T, Coda A, et al. Increased serine protease activity and cathelicidin promotes skin inflammation in rosacea. Nat Med 2007;13:975−80.

Yamasaki K, Gallo RL. Rosacea as a disease of cathelicidins and skin innate immunity. J Investig Dermatol Symp Proc 2011;15:12−5.

Yokouchi M, Kubo A, Kawasaki H, Yoshida K, Ishii K, Furuse M, et al. Epidermal tight junction barrier function is altered by skin inflammation, but not by filaggrin-deficient stratum corneum. J Dermatol Sci 2015;77: 28−36.

Zhang X, Yin M, Zhang LJ. Keratin 6, 16 and 17-critical barrier alarmin molecules in skin wounds and psoriasis. Cells 2019;8.

SUPPLEMENTARY MATERIALS AND METHODS

Patients and healthy controls

Skin punch biopsies (0.5—1 cm^2) were taken from lesional facial skin of eight patients with papulopustular rosacea and from sebaceous gland—rich (SGR) skin of eight healthy individuals after obtaining written informed consent, according to the Declaration of Helsinki principles (Supplementary Table S4). The study was approved by the local ethics committee of University of Debrecen, Hungary.

Processing of skin biopsy specimens

All biopsies were cut into two pieces. For immunohistochemistry, samples were formalin-fixed and paraffin-embedded, and for quantitative RT-PCR, samples were stored in RNAlater (Qiagen, Hilden, Germany) at −70 °C until RNA isolation.

RNA isolation and reverse transcription

All samples were homogenized in Tri reagent solution (Sigma-Aldrich, St. Louis, MO) with Tissue Lyser (Qiagen) using previously autoclaved metal beads (Qiagen). The concentration and purity of the RNA were measured by means of NanoDrop spectrophotometer (Thermo Fisher Scientific, Bioscience, Waltham, MA), and its quality was checked using an Agilent 2100 bioanalyzer (Agilent Technologies, Santa Clara, CA). For RT-PCR, cDNA was synthesized from the isolated RNA using the High Capacity cDNA Archive Kit (Invitrogen, Life Technologies, Carlsbad, CA).

RT-qPCR

RT-PCR was carried out in triplicate using pre-designed MGB assays ordered from Applied Biosystems (Life Technologies).

The following TaqMan Gene Expression assays were used: PPIA (Hs99999904_m1), FLG (Hs00856927_g1), KRT1 (Hs00196158_m1), KRT6A (Hs01699178_g1), KRT10 (Hs00166289_m1), KRT16 (Hs00373910_g1), KRT17 (Hs00356958_m1), LCE1D (Hs04224967_gH), LCE1F (Hs00820275_sH), LOR (Hs01894962_s1), CLDN1 (Hs00221623_m1), CLDN16 (Hs00198134_m1), CLDN23 (Hs01013638_s1), OCLN (Hs00170162_m1), CDH1 (Hs01023895_m1), DSC1 (Hs00245189_m1), CDSN (Hs00169911_m1), DSG1 (Hs00355084_m1), TGM1 (Hs00165929_m1), TGM3 (Hs00162752_m1), TGM5 (Hs00909973_m1), KLK5 (Hs01548153_m1), KLK7 (Hs00192503_m1), KLK14 (Hs00983577_m1), SPRR1A (Hs00954595_s1), SPRR2A (HS03046643_s1), ABCA12 (Hs00292421_m1), PKP1 (Hs00240873_m1), S100A7 (Hs00161488_m1), S100A8 (Hs00374264_g1), S100A9 (Hs00610058_m1), LCN2 (Hs01008571_m1), DEFB4B (hBD-2) (Hs00175474_m1), TSLP (Hs00263639_m1), and LL37 (CAMP) (Hs00189038_m1). All reactions were performed with an ABI PRISM 7000 Sequence Detection System. Relative mRNA levels were calculated using the 2-ΔΔCt method normalized to the expression of PPIA mRNA.

RNA sequencing (RNASeq) analysis

Complementary DNA library for RNASeq was generated from 1 μg total RNA using TruSeq RNA Sample Preparation Kit (Illumina, San Diego, CA) according to the manufacturer's protocol. Briefly, poly-A tailed RNAs were purified by oligodT-conjugated magnetic beads and fragmented on 94 °C for 8 minutes, then first strand cDNA was transcribed using random primers and SuperScript II reverse transcriptase (Life Technologies). Following this step, second strand cDNA was synthesized, double-stranded cDNA was end repaired and 3′ ends adenylated, and Illumina index adapters were ligated. After adapter ligation enrichment, PCR was performed to amplify adapter ligated cDNA fragments. Fragment size distribution and molarity of libraries were checked on Agilent BioAnalyzer DNA1000 chip (Agilent Technologies, Santa Clara, CA). Concentrations of RNASeq libraries were set to 10 nM and five libraries were pooled together before sequencing. A single read 50 base pair sequencing run was performed on Illumina HiScan SQ instrument (Illumina), and 16—18 million reads per sample were obtained. CASAVA software was used for pass filtering and demultiplexing process. Sequenced reads were aligned to Human Genome v19 using TopHat and Cufflinks algorithms and bam files were generated. StrandNGS software was used for further statistical analysis. Bam files were imported and normalized using DESeq algorithm. To identify statistically significant gene expression patterns between conditions, nonparametric Wilcoxon—Mann—Whitney test was used.

Library preparations, sequencing, and data analysis were performed at the Genomic Medicine and Bioinformatics Core Facility of University of Debrecen.

A part of our RNASeq data (SGR1—SGR6 samples) has been previously published and deposited to the Sequence Read Archive database (https://www.ncbi.nlm.nih.gov/sra), under accession number PRJNA421246, whereas SGR7, SGR8, and PPR1—PPR8 samples are available in the Sequence Read Archive database (https://www.ncbi.nlm.nih.gov/sra), under accession number PRJNA592080.

Pathway analyses

To identify the function of the aforementioned differentially expressed genes (DEGs), multiple bioinformatics analyses were performed by Cytoscape ClueGO bioinformatics tool using Gene Ontology Biological Process, Immune System Process, and Molecular Function; Kyoto Encyclopedia of Genes and Genomes and Kyoto Encyclopedia of Genes and Genomes Compound; Reactome Pathways; and Reactome Reactions databases.

First, to identify the general biological function of DEGs, we performed a pathway enrichment analysis on all DEGs with fold change ≥ 1.5. To reveal the significantly enriched ($P \leq 0.05$) terms and pathways, the following criterion was applied: all terms should have contained at least 50 genes from our input gene set.

Then, we performed a second, stricter pathway enrichment analysis to find out the function of barrier-related significant DEGs with fold change ≥ 1.5 in more detail; thus, a different analytical approach was applied. Up- and downregulated DEGs were subjected as two different clusters to a more detailed pathway enrichment analysis by ClueGO. According to the fact that most DEGs were upregulated (approximately 61%), the criteria of the analysis were different in the cases of up- and downregulated gene sets. Regarding the cluster of upregulated genes, terms should have contained at least 30 genes from our input gene set and at least 20% of all genes characteristic to each term, whereas the cluster of downregulated genes required at least 18 genes from our input

gene set and at least 12% of all genes characteristic to each term. This approach allowed us not only to reveal significantly enriched specific terms and pathways but also made us capable of easily distinguishing and visualizing up- and downregulated DEGs belonging to each terms. Regarding the statistical approach of the enrichment analyses by Cytoscape, a P-value < 0.05 and kappa coefficient of 0.4 were considered as threshold values and correction was performed by Benjamini—Hochberg test.

Immunohistochemistry

For immunohistochemistry analyses, paraffin-embedded sections from patients and healthy controls were deparaffinized. Heat-induced antigen retrieval was performed, and sections were preprocessed with H_2O_2 for 10 minutes. Sections were stained with primary antibodies against human CDSN (rabbit polyclonal IgG [HPA054184], Sigma-Aldrich), human CLDN1 (rabbit polyclonal IgG [ab15098], Abcam, Cambridge, United Kingdom), human DSG1 (rabbit polyclonal IgG [NBP1-84567], Novus Biologicals, Centennial, CO), human FLG (mouse monoclonal IgG [ab218862], Abcam), human KRT1 (rabbit monoclonal IgG [ab185628], Abcam), human KRT6 (mouse monoclonal IgG [ab18586], Abcam), human lipocalin/NGAL (rabbit polyclonal IgG [PA5-32476], Invitrogen), human LOR (rabbit monoclonal IgG [NBP133610], Novus Biologicals), human S100A8 (rabbit polyclonal IgG [PA532476], Invitrogen), and human TGM5 (rabbit polyclonal IgG [ab133786], Abcam).

Subsequently, the following horseradish peroxidase—conjugated secondary antibodies were employed: anti-mouse/rabbit (Biogenex, Fremont, CA). Before and after incubating with antibodies, washing of samples was performed for 5 minutes, 3 times in each step. Staining was detected with the Vector NovaRed Kit (Vector Laboratories, Burlingame, CA). Sections were counterstained with methylene green, dehydrated, and covered with a glass coverslip. The detection of one protein was carried out on all sections in parallel at the same time to enable us to evaluate comparable protein levels. Positive, Ig, and isotype controls were also used to normalize staining against all proteins (mouse IgG2a Kappa [Covalab, Villeurbanne, France] and rabbit immunoglobulin fraction [Sigma-Aldrich]).

The sections were digitized using Whole Slide Imaging technology in the Department of Pathology, and the Pannoramic Viewer software was used for the evaluation of the degree of staining of the slides.

Statistical analysis

Data distribution was analyzed by Kolmogorov-Smirnov test. Because our data showed normal distribution, two groups of samples were compared statistically by two-sample t-test. Differences between the groups were demonstrated using mean $\pm$ 95% confidence interval. P-values < 0.05 were considered statistically significant (*$P < 0.05$; **$P < 0.01$; ***$P < 0.001$). Statistical data was analyzed using GraphPad Prism v6 (GraphPad Software Inc., La Jolla, CA) and SPSS 25 (SPSS package for Windows, Chicago, IL).
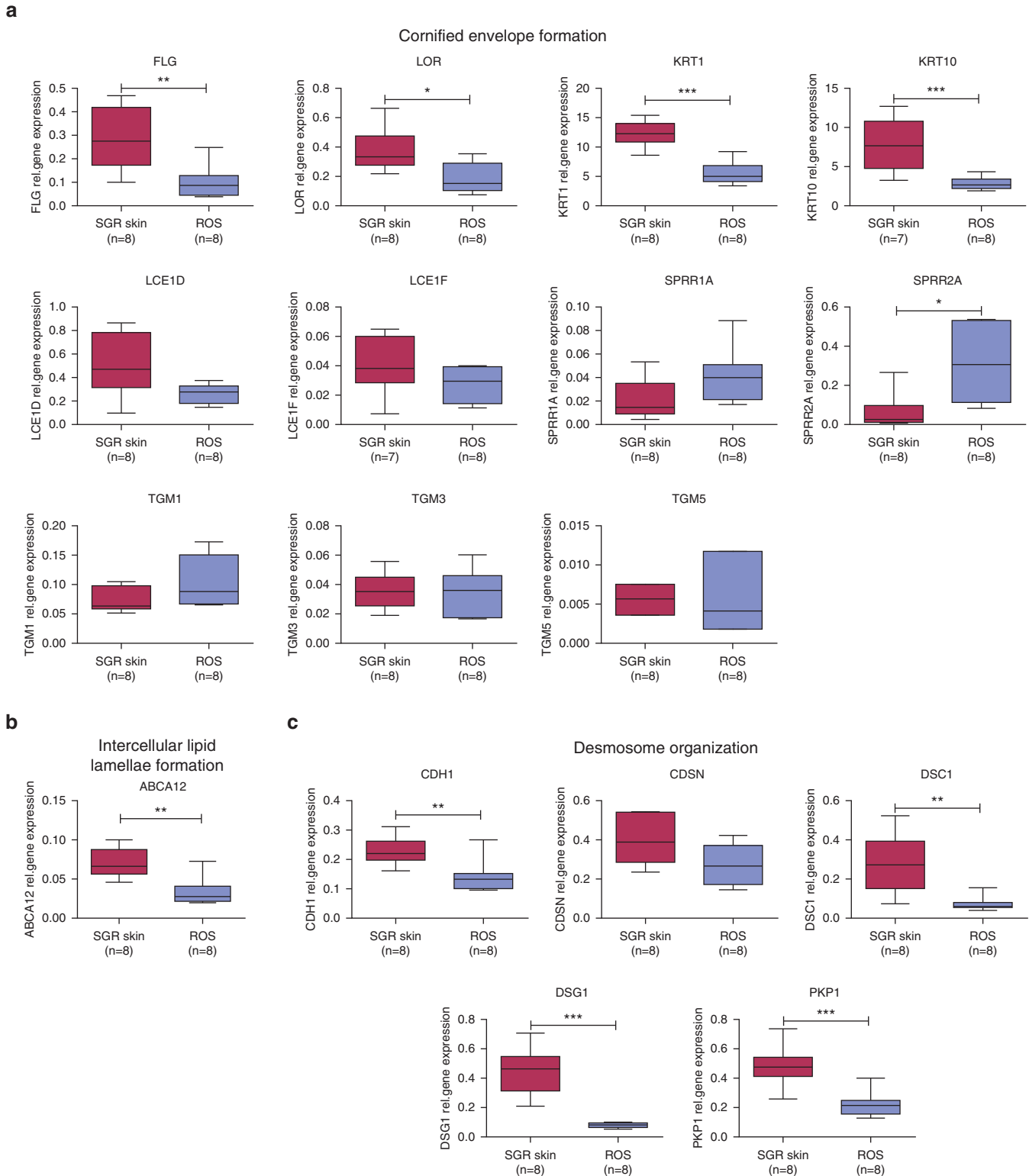
Supplementary Figure S1. Significantly altered expression of the components of cornified envelope, intercellular lamellae formation, and desmosome organization in ROS examined by qRT-PCR. (**a**) Cornified envelope. (**b**) Intercellular lamellae formation. (**c**) Desmosome organization. The graphs show the mean ± 95% confidence interval of measured mRNA transcript levels (*$P < 0.05$; **$P < 0.01$; ***$P < 0.001$, as determined by two-sample *t*-test). CDSN, corneodesmosin; DSG1, desmoglein 1; ROS, papulopustular rosacea; SGR, sebaceous gland−rich.
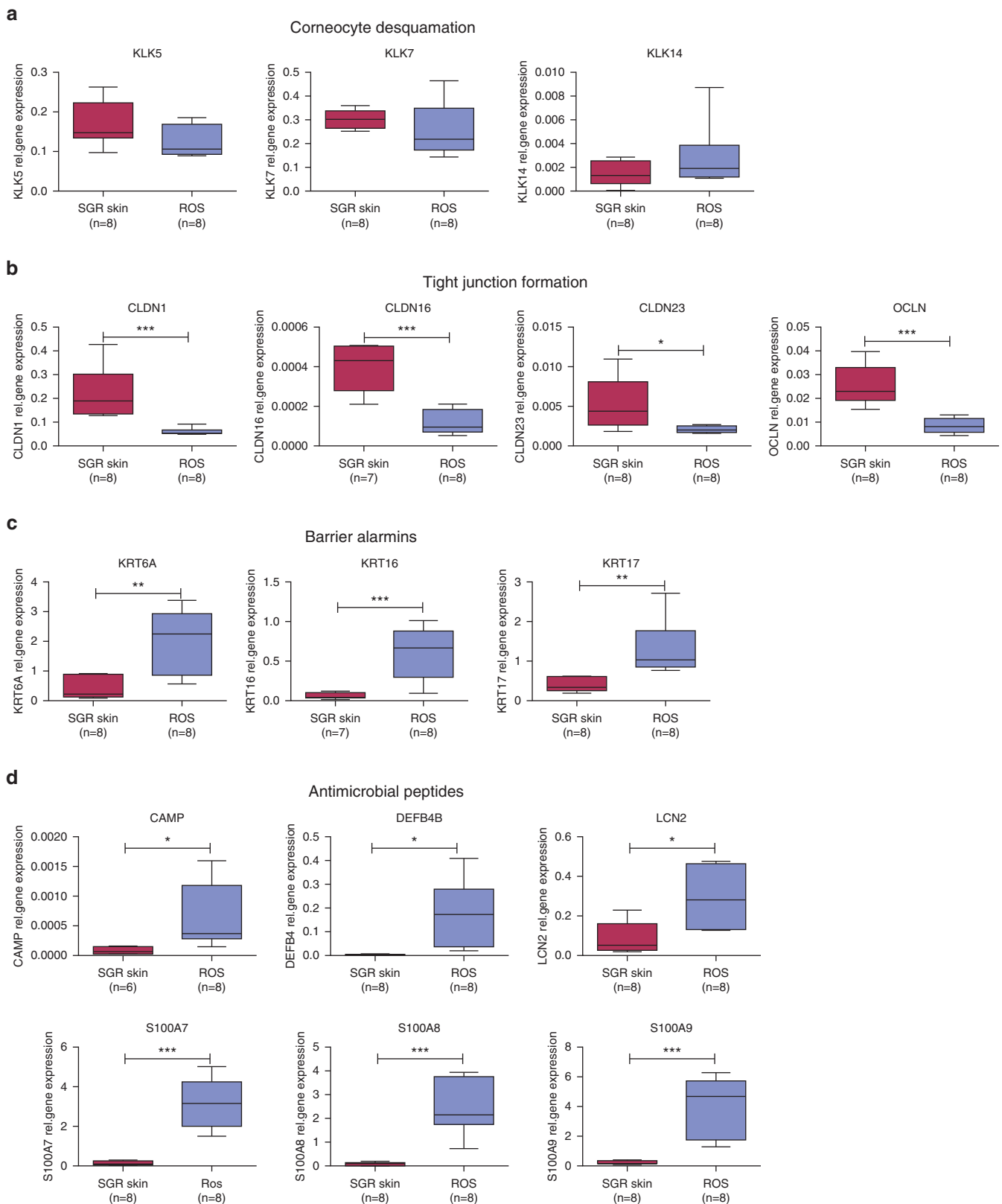
Supplementary Figure S2. Significantly altered expression of the components of corneocyte desquamation, tight junctions, barrier alarmins, and antimicrobial peptides in ROS examined by qRT-PCR. (**a**) Corneocyte desquamation. (**b**) Tight junctions. (**c**) Barrier alarmins. (**d**) Antimicrobial peptides. The graphs show the mean ± 95% confidence interval of measured mRNA transcript levels (*$P < 0.05$; **$P < 0.01$; ***$P < 0.001$, as determined by two-sample *t*-test). CAMP, cathelicidin; ROS, papulopustular rosacea; SGR, sebaceous gland–rich.

Supplementary Table S4. Characteristics of the Studied Skin Samples of Healthy Controls and Patients with PPR

SGR skin samples (n = 8)

Healthy individuals	Sex	Age	Localization
SGR1	F	77	Hairy scalp
SGR2	M	62	Mandibula
SGR3	F	57	Nose
SGR4	F	61	Nose
SGR5	F	42	Scapula
SGR6	F	38	Chin
SGR7	M	47	Face
SGR8	M	66	Face
Mean age ± SD		56.25 ± 13.11	

Rosacea skin samples (n = 8)

PPR individuals	Sex	Age	Localization
PPR1	F	36	Forehead
PPR2	F	53	Nose
PPR3	F	60	Chin
PPR4	M	79	Nose
PPR5	M	71	Nose
PPR6	F	69	Forehead
PPR7	F	57	Forehead
PPR8	F	50	Chin
Mean age ± SD		59.38 ± 13.59	

Abbreviations: F, female; M, male; PPR, papulopustular rosacea; SGR, sebaceous gland–rich.